International Journal of Fracture **51**: 121–138, 1991.
Z.P. Bažant (ed.), Current Trends in Concrete Fracture Research.

Size dependence of concrete fracture energy determined by RILEM work-of-fracture method

ZDENĚK P. BAŽANT and MOHAMMAD T. KAZEMI
Center for Advanced Cement-Based Materials, Northwestern University, Evanston, Illinois, 60208, USA

Received 1 June 1990; accepted 1 November 1990

Abstract. The paper analyzes the size dependence of the fracture energy of concrete obtained according to the existing RILEM recommendation proposed by Hillerborg and based on the work-of-fracture method of Nakayama, Tattersal and Tappin, in which the energy dissipated at the fracture front is evaluated from the measured load-displacement curve. The analysis is based on the size effect law proposed by Bažant, which has been shown to be applicable to the size ranges up to about 1:20 and apply in the same form for all specimen geometries. The analysis utilizes the previously developed method for calculating the R-curve from the size effect, and the load-deflection curve from the R-curve. The R-curve is dependent on the geometry of the specimen. The results show that the fracture energy according to the existing RILEM recommendation is not size-independent, as desired, but depends strongly on the specimen size. This dependence is even stronger than that of the R-curve. When the specimen size is extrapolated to infinity, the fracture energy according to the RILEM recommendation coincides with the fracture energy obtained by the size effect method. It is also found that, in fracture specimens of usual sizes, the pre-peak contribution of the work of the load to the fracture energy is relatively small. Finally, as a by-product, the analysis also verifies the fact that, in three-point bend fracture specimens, the fracture energy according to the RILEM definition is dependent on the notch depth.

1. Introduction

Since concrete is a brittle heterogeneous material in which fracture is preceded by a large fracture process zone of variable size, determination of the fracture energy of concrete, G_f, is not an easy matter. The only unambiguous definition of fracture energy can be given in terms of an extrapolation of the specimen size to infinity [1–2]. This definition of course requires knowledge of the size effect law for fracture. Its exact form is not known, but an approximate size effect law for the nominal stress at failure that is sufficient for most practical purposes has recently been established [1–4]. When the existing RILEM recommendation for the measurement of fracture energy of concrete was formulated [5–6], the size effect law for fracture had not yet been known. The fracture energy was in that recommendation defined according to the work-of-fracture method, originally proposed by Nakayama [7], and by Tattersall and Tappin [8] (the latter authors also discovered size effect in this method). Adoption of the work-of-fracture method for concrete was recommended by Hillerborg and co-workers [6, 9–10] on the basis of their work as well as earlier studies of concrete (e.g. [10–12]).

Based on a measured load-deflection curve of a fracture specimen, typically a three-point-bend beam, the work of load P (including the effect of its own weight) on the load-point displacement u is, in the RILEM method, calculated as

$$W_f = \int_0^{u_f} P\,du, \tag{1}$$

in which u_1 = final displacement at which the load is reduced to zero. The fracture energy according to the RILEM definition, G_f^R, represents the average (or effective) fracture energy in the ligament [7, 11]. It is obtained as [5–6, 9–10]:

$$G_f^R = W_f/bl, \quad l = (1 - \alpha_0)d, \tag{2}$$

in which l = length of ligament, d = depth of the beam, $\alpha_0 = a_0/d$, a_0 = length of notch, b = thickness of the beam (Fig. 1), and bl = effective area of fractured ligament. However, as we will see, the averaged value depends considerably on the specimen size as well as shape. Such differences would have to be minor if the fracture process zone (or cohesive zone, bridging zone) were very small compared to the ligament length. However, this is not the case in fracture testing of concrete (except if impractically large specimens were used).

The RILEM definition is based on Hillerborg's fictitious crack model [6, 10, 13] and previous similar models for other materials (e.g. [14]) in which it has been tacitly assumed that the crack bridging stress σ_b in the cohesive zone (or fracture process zone) is a function of the crack opening displacement δ but no other variable, i.e. that the relation of σ_b and δ is unique. If this hidden hypothesis were true, then (2) would have to be exact, independent of specimen size, because the total energy dissipated along the ligament (i.e. $\int_0^\infty \sigma_b \, d\delta$) would be uniform (as the complete curve $\sigma_b(\delta)$, down to zero σ_b, has been traced at every point of the ligament by the time of complete fracture). As we will see, however, this hypothesis cannot be true. In fact there is no reason to expect the path $\sigma_b(\delta)$ not to depend on the normal strains parallel to the crack plane, on the deformation state in a small neighborhood of the point, and on the deformation history.

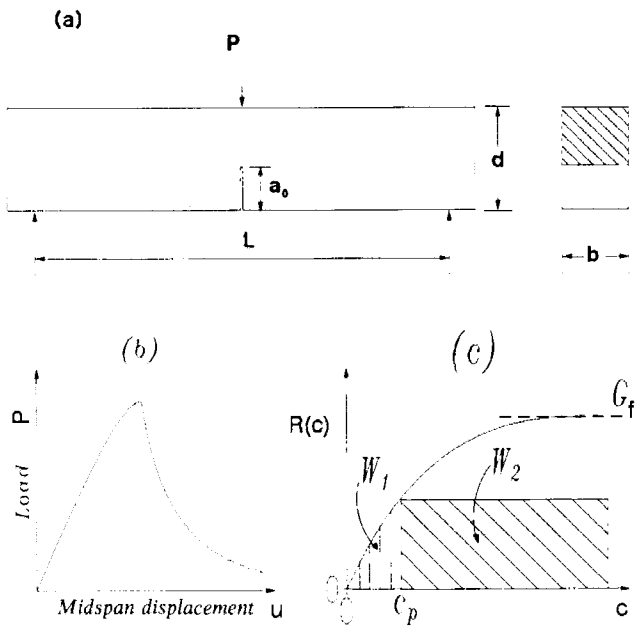

Fig. 1. Three-point bend specimen geometry, load deflection curve, *R*-curve and subdivision of work according to the *R*-curve.

Note that the fictitious crack model does not imply the energy release rate G for the elastically equivalent sharp crack to be constant during crack propagation. The reason is that, unless the fracture front is remote from both the notch tip and specimen boundaries, the σ_b-distribution throughout the cohesive zone varies during propagation, giving different values for G; $G = \int_0^l \sigma_b[\delta(x)](\mathrm{d}\delta(x)/da]\,\mathrm{d}x$ where x is the coordinate along the ligament measured from the notch tip, and $\mathrm{d}\delta/da = (\mathrm{d}\delta/\mathrm{d}t)/(da/\mathrm{d}t)$ where t = time and a = depth of effective (elastically equivalent) crack (which gives the same specimen compliance).

As a variant of the RILEM method, the fracture energy can also be measured by fracturing the specimen only partially. In this procedure, which usually involves unloading in the softening zone [15], the measured work (partial work-of-fracture) is divided by the area of the advancing crack, which needs to be somehow measured or estimated. As another variant, some researchers used cyclic testing for calculation of the fracture energy as a function of crack length [16–17]. In this method, the partial works-of-fracture between any two consecutive cycles are divided by the corresponding areas of crack advance. It needs to be noted, however, that the loading rate [17–18] and creep of course affect the work-of-fracture. This effect is greater in cyclic than monotonic tests. Moreover, cyclic loading no doubt produces inelastic volume dilatancy and residual stress in the fracture process zone, which are absent in monotonic tests.

Various series of experiments have demonstrated that G_f^R is significantly size and shape dependent [8–9, 17–32]. Planas, Elices, and co-workers [28–30] attempted to extrapolate the values of G_f^R to infinite size ($G_f^P = \lim G_f^R$ for $d \to \infty$), using a simple and approximate size effect relation, which they called the perturbed ligament model:

$$G_f^R = G_f^P \frac{l - l_p}{l}, \tag{3}$$

where l_p = a size-independent constant called the perturbation length (which depends on material properties as well as geometry), and l = ligament length, which appears to be a few-times larger than l_p. Equation (3) is treated as independent of specimen geometry, although this cannot be exactly so since otherwise two different specimens of the same l, e.g. three-point-bend and wedge-splitting specimens, would have to yield the same fracture energy. Parameters G_f^P and l_p can be obtained by linear regression analysis. Planas, Elices, and co-workers [28–30] concluded that the fracture energy values so obtained appear to be unambiguous, and that G_f^P needs to be determined from a set of tests of specimens of different sizes, with a sufficient size range, similar to the size effect method proposed by Bažant [1, 2].

The purpose of this study is to analyze the size dependence of G_f^R on the basis of the size effect law proposed by Bažant [3] for the nominal strength at failure. This has recently been shown to have a relatively broad validity, being applicable to the size range up to about 1:20, and to be rather insensitive to the specimen shape (geometry).

2. Review of size effect law

The most important consequence of fracture mechanics is the effect of size on the nominal strength (i.e. nominal stress at maximum load). To describe it, we consider geometrically similar

structures (or specimens) of different sizes (with geometrically similar notches or initial cracks), and introduce the nominal strength

$$\sigma_N = c_n \frac{P_u}{bd}, \tag{4}$$

where P_u = maximum load (ultimate load), b = thickness of two-dimensionally similar structures or specimens (which should best be chosen the same for test specimens of all the sizes), d = characteristic dimension of the structure or specimen, and c_n = coefficient introduced for convenience.

Plastic limit analysis, as well as elastic analysis with an allowable stress criterion or any failure criterion based on stress or strain, is known to exhibit no size effect, i.e., geometrically similar structures of different sizes fail at the same σ_N. However, this is not true in fracture mechanics. Due to similarity of stress fields in similar two-dimensional elastic structures of different sizes, the total potential energy of the structure must have the form $U = (\sigma^2/2E')Vf(\alpha)$ where $\sigma = c_n P/bd$, P = load; $V = bd^2$ = measure of volume; $f(\alpha)$ is a function of the relative crack length $\alpha = a/d$ (a is the crack length) and depends on the shape of the structure; $E' = E$ for plane stress, $E' = E/(1 - \nu^2)$ for plane strain, E = Young's modulus of elasticity, and ν = Poisson's ratio. Therefore, the energy release rate is $G = -(\partial U/\partial a)/b = -(\partial U/\partial \alpha)/bd = -(\sigma^2/2E')f'(\alpha)d$, from which

$$G = \frac{P^2 g(\alpha)}{E' b^2 d}, \quad K_{\mathrm{I}} = \sqrt{GE'} = \frac{Pk(\alpha)}{b\sqrt{d}}, \tag{5}$$

where $f'(\alpha) = \partial f(\alpha)/\partial \alpha$, $g(\alpha) = -f'(\alpha)c_n^2/2$, and $k(\alpha) = \sqrt{g(\alpha)}$. The values of $g(\alpha)$ can be obtained by linear elastic analysis, such as elastic finite element analysis. For basic specimen geometries, $k(\alpha)$ also follows from the formulas for the stress intensity factors found in handbooks (e.g. Tada et al. [33]).

In materials with toughening mechanisms, such as rock, concrete, ice and ceramics, there is a large fracture process zone in front of the continuous crack. The maximum loads for various sizes may be assumed to occur when the tip of the equivalent elastic crack is at a certain distance c ahead of the tip of the initial crack or notch, i.e., $a = a_0 + c$ or $\alpha = \alpha_0 + c/d$ where $\alpha_0 = a_0/d$, and a_0 = initial crack or notch length. We assume that G cannot decrease and consider G_f to be the maximum value of G as $d \to \infty$. The corresponding maximum possible value of c at peak load, obtained for $d \to \infty$ (and $G \to G_f$), is denoted as c_f.

The fracture process zone starts with zero size and then grows as the loading increases while remaining attached to the notch tip (provided that the specimen geometry is such that $g'(\alpha) > 0$, which is the case for the three-point-bend specimen). The value of G required for fracture growth is basically determined by the size of the process zone. Since the value of c is also determined by this size, the value of G is directly related to the corresponding value of c. The magnitude of c at $P = P_u$ fully determines the value of α and, consequently, the value of $g(\alpha)$. So the ratio $G/g(\alpha)$ at $P = P_u$ for any specimen size should be approximately equal to $G_f/g(\alpha_1)$ where α_1 corresponds to c_f in a specimen of any size d, i.e. $\alpha_1 = (a_0 + c_f)/d = \alpha_0 + c_f/d$. Therefore, at $P = P_u$, we have $G = G_f g(\alpha)/g(\alpha_1)$. We may now substitute this expression into (5) along with $P_u \simeq \sigma_N \mathrm{bd/c}_n$ and $g(\alpha_1) \simeq g(\alpha_0) + g'(\alpha_0)c_f/d$ (which

ensues from Taylor series expansion assuming that $g'(\alpha_0) > 0$). Then, solving for σ_N, we obtain the size effect law [34]

$$\sigma_N = c_n\left(\frac{E'G_f}{g'(\alpha_0)c_f + g(\alpha_0)d}\right)^{1/2}. \tag{6}$$

Equation (6) may alternatively be written as [34–35]

$$\tau_N = \left(\frac{E'G_f}{c_f + \bar{d}}\right)^{1/2}, \tag{7}$$

where $\tau_N = \sqrt{g'(\alpha_0)}P_u/bd$, $\bar{d} = \mathrm{dg}(\alpha_0)/g'(\alpha_0)$; τ_N = intrinsic nominal stress at failure, and $\bar{d}$ = intrinsic size of the structure, which are both independent of the specimen shape. The quantity that makes them shape-independent is the factor $g(\alpha_0)/g'(\alpha_0)$ [34], which has also been introduced for similar purposes by Planas and Elices [36] and for other purposes by Horii et al. [37].

Although the foregoing derivation [34] involves certain simplifications, other completely different arguments, including (1) dimensional analysis and similitude [3–4, 1], (2) simplified energy release considerations [3], and (3) deterministic limit of nonlocal generalization of Weibull-type statistical theory of strength [38], have been shown to yield the same result in a more general form:

$$\sigma_N = \frac{Bf_u}{\sqrt{1+\beta}}, \quad \beta = \frac{d}{d_0}, \tag{8}$$

where f_u is a measure of material strength, B and d_0 are two empirical constants. This is equivalent to (6) if $B = c_n[E'G_f/c_f g'(\alpha_0)]/f_u$ and $d_0 = c_f g'(\alpha_0)/g(\alpha_0)$. Taking the limit of (5) in which $P = P_u = \sigma_N bd/c_n$, expressing σ_N from (8), and noting that $\lim \alpha \to \alpha_0$ for $d \to \infty$, one gets the formula [1]

$$G_f = \frac{B^2 f_u^2 d_0 g(\alpha_0)}{c_n^2 E'}. \tag{9}$$

Parameter B characterizes σ_N of very small structures and can be determined as $B = c_n P_u/f_u bd$ (from (8) for $\beta \to 0$), where P_u is calculated by plastic limit analysis. In the case that G_f is known the other parameter of the size effect law (d_0 in (8)) can be obtained from (9).

Parameter β in (8), called the brittleness number [1, 2], may be expressed as [34–35] either

$$\beta = \frac{B^2 f_u^2 g(\alpha_0)d}{c_n^2 E'G_f} \tag{10a}$$

or

$$\beta = \frac{g(\alpha_0)d}{g'(\alpha_0)c_f} = \frac{\bar{d}}{c_f}. \tag{10b}$$

Since (10a) involves the value of B that characterizes the peak load of a small structure, this equation is more accurate when β is small. On the other hand, (10b), based on (6), is more accurate when β is large since it is based solely on LEFM approximation.

Other definitions of the brittleness number were proposed by Homeny et al. [39], Carpinteri [40] and Hillerborg [6]. However, they only permit comparing specimens of different sizes but the same shape, and do not represent universal (shape-independent) measures of brittleness.

In an infinitely large specimen, the fracture process zone occupies only an infinitesimal volume fraction of the body, and so the body can be treated as elastic. Consequently, the stress and displacement fields surrounding the fracture process zone are the asymptotic elastic fields. They are known to be the same for any specimen geometry, and so there can be no influence of the shape of the boundary on the fracture process zone. It follows that G_f and c_f in an infinitely large specimen are independent of the specimen shape. Therefore, unambiguous definitions of G_f and c_f as fundamental material properties, independent of specimen size and shape, can be given as follows [1, 34, 36]: G_f and c_f are the energy required for crack growth and the elastically equivalent length of the fracture process zone, respectively, in an infinitely large specimen.

This definition of fracture energy can be mathematically stated as $G_f = \lim G_c = \lim(K_{Ic}^2/E')$ for $d \to \infty$, where G_c and K_{Ic} are the values of G and K_I (5), respectively, calculated for the measured peak load P_u and initial crack or notch length a_0 using linear elastic fracture mechanics. (More generally, one could define $G_f = \lim J$ for $d \to \infty$ where J is Rice's J-integral.)

For certain specimen geometries (for example, the center-notched panel loaded on the crack, the double cantilever specimen, the identation fracture test, the double-punch compression test and various chevron-notched specimens), $g'(\alpha)$ can be negative for some values of α and $g(\alpha)$ attains a minimum at a certain value, α_{min} [7–8, 15–17, 41–43]. In these cases, the peak load for ideally brittle materials (having no fracture process zone) occurs when α equals the value of α_0 or α_{min}, whichever is larger. When $g'(\alpha)$ is negative, the crack propagation is to a certain extent stable even under load control. The tests are, therefore, easier to control than the tests in which $g'(\alpha)$ is positive. These observations have lead various investigators to expect the toughness value obtained from the peak load of a test where $g'(\alpha_0)$ is initially negative to be size-independent, and therefore a true material property. Later, however, several investigators [42–43] observed that the fracture toughness values computed from this type of tests are size-dependent. The reason is that the equivalent relative crack length at the peak load depends strongly on the size, and is greater than both α_{min} and α_0. (It may be noted that, on the micro- or meso-scale, negativeness of $g'(\alpha)$ explains the observed stability of microcracking [44].)

In conventional testing, the apparent fracture energy, G_c, is usually determined by methods of linear elastic fracture mechanics without regard to the variations of the size of the fracture process zone, as if $\alpha = \alpha_0$ ($a = a_0$, $c = 0$) at failure. For that case, one gets (from (5)) $G_c = P_u^2 g(\alpha_0)/E'b^2 d$, which is size dependent. Substituting $P_u^2 = (\sigma_N bd/c_n)^2 = (Bf_u bd/c_n)^2 d_0/(d + d_0)$ and expressing Bf_u by using G_f from (9), one gets

$$G_c = \tau_N^2 \bar{d} = G_f \frac{d}{d + d_0} = G_f \frac{\bar{d}}{\bar{d} + c_f} = G_f \frac{\beta}{\beta + 1}. \tag{11}$$

The ratio $\beta_s = G_c/G_f = \beta/(1 + \beta)$, based on fracture energy [39], (as well as any other smooth monotonic function of β) could alternatively also be considered as a brittleness number; β_s varies from zero to one as the size increases from zero to infinity. According to (8), the size sensitivity of nominal strength [6] can be characterized by $(\Delta\sigma_N/\sigma_N)/(\Delta d/d) = -\beta_s/2$ or $\beta_s = -2(\Delta\sigma_N/\sigma_N)/(\Delta d/d)$.

Since $K_{Ic} = \sqrt{EG_c}$, the apparent fracture toughness is found [2] to vary as

$$K_{Ic} = \tau_N \bar{d}^{1/2} = K_{If}\left(\frac{\bar{d}}{\bar{d} + c_f}\right)^{1/2} = K_{If}\left(\frac{\beta}{1 + \beta}\right)^{1/2}. \tag{12}$$

These expressions follow from (6) and (7), and fracture toughness K_{If} is the value of K_{Ic} for an infinitely large specimen, corresponding to G_f, i.e. $K_{If} = \sqrt{E'G_f}$, which is a constant.

The size effect law has the advantage that its parameters G_f (or K_{If}) and c_f can be determined from the measured peak loads P_u by linear regression [3]. Algebraic rearrangement of (7) and (12) yields the linear plots

$$Y = AX + C \quad \text{or} \quad Y' = A'X' + C', \tag{13}$$

in which

$$X = \bar{d}, \quad Y = 1/\tau_N^2, \quad A = 1/K_{If}^2, \quad C = c_f/K_{If}^2, \tag{14}$$

$$X' = 1/\bar{d}, \quad Y' = 1/K_{Ic}^2, \quad A' = c_f/K_{If}^2, \quad C' = 1/K_{If}^2. \tag{15}$$

Each plot yields the slope of the regression line and its vertical intercept, from which the values of c_f and K_{If} follow. To make sure the size range of the specimens has been sufficient, one must use the well-known formulas of regression statistics for the coefficient of variation of the regression slope, and check whether its value is small enough [2].

3. Determination of *R*-curve and calculation of the load-displacement curve

The fracture process zone ahead of the notch is created by various mechanisms such as microcracking and bridging [37, 44–46]. The size of the fracture process zone grows as the fracture propagates [15, 23, 47]. This is manifested as an increase of the resistance $R(c)$ to fracture growth, representing the energy dissipated per unit length of fracture extension and unit width. As shown in [48], and refined in [34], the R-curve can be calculated from the material parameters obtained by size effect

$$R(c) = G_f \frac{g'(\alpha)}{g'(\alpha_0)} \frac{c}{c_f}, \tag{16}$$

in which

$$\frac{c}{c_f} = \frac{g'(\alpha_0)}{g(\alpha_0)}\left(\frac{g(\alpha)}{g'(\alpha)} - \alpha + \alpha_0\right). \tag{17}$$

These equations define the R-curve parametrically. After determining G_f and c_f from the size effect law, a series of α-values may be chosen and for each of them the length c of an elastically equivalent traction-free crack calculated from (17), and then $R(c)$ determined from (16). If c is specified, α may be solved by Newton iterations and subsequently $R(c)$ computed. The R-curve obtained according to (16) depends on specimen geometry.

For readers' convenience, the derivation of (16) and (17) is briefly as follows [34]. The energy balance at failure requires that $F(c, d) = G(\alpha, d) - R(c) = 0$ where $\alpha = a/d = \alpha_0 + c/d$. If we change the size slightly from d to $d + \delta d$ but keep the geometric shape (i.e. $\alpha_0 =$ constant), failure now occurs at $c + \delta c$, and since $G = R$ must hold also for $c + \delta c$, we must have $\partial F/\partial d = 0$. Geometrically, the condition $\partial F/\partial d = 0$ together with $F(c, d) = 0$ means that the R-curve is the envelope of the family of fracture equilibrium curves $F(c, d) = 0$ for various sizes d [48]. Because the R-curve is size-independent, we have $\partial R/\partial d = 0$ and so $\partial G/\partial d = 0$. Now we may substitute $P_u^2 = (\sigma_N bd/c_n)^2 = (Bf_u bd/c_n)^2/(1 + d/d_0)$ where $(Bf_u)^2 = c_n^2 E' G_f/d_0 g(\alpha_0)$ (according to (9)) into $G = P_u^2 g(\alpha)/E' b^2 d$ (5). We thus obtain for the critical states

$$G(\alpha, d) = G_f \frac{g(\alpha)}{g(\alpha_0)} \frac{d}{d + d_0}. \tag{18}$$

Substituting this into $\partial G/\partial d = 0$, differentiating, and noting that $\partial\alpha/\partial d = \partial\alpha_0/\partial d + \partial(c/d)/\partial d = -c/d^2 = -(\alpha - \alpha_0)/d$ (because $\partial\alpha_0/\partial d = 0$ for geometrically similar structures), we get

$$\beta = \frac{d}{d_0} = \frac{g(\alpha)}{(\alpha - \alpha_0)g'(\alpha)} - 1. \tag{19}$$

Furthermore, substituting this, along with the relations $(\alpha - \alpha_0)d = c$ and $d_0 = d/\beta = c_f g'(\alpha_0)$ (from (10b)) into (18), and setting $G(\alpha, d) = R(c)$, (16) and (17) are proven.

The dependence of the fracture toughness on c (i.e. the R-curve of fracture toughness) can be determined from the relation $K_{IR} = \sqrt{E'R}$:

$$K_{IR} = K_{If}\left(\frac{k(\alpha)k'(\alpha)c}{k(\alpha_0)k'(\alpha_0)c_f}\right)^{1/2}. \tag{20}$$

Equation (16) or (20) applies only as long as the fracture process zone grows and remains attached to the notch tip, which is approximately up to the peak load. The behavior for the post-peak regime will be discussed later.

The fact that the R-curves depend on the size of the specimen as well as its geometry (including the notch length) has been observed experimentally [31, 49–50]. It may also be noted that, according to some tests [50], interaction of the fracture process zone with the specimen boundary can even lead to a falling R-curve after a plateau is passed; however, the declining part of the R-curve is significant only for specimens with very small uncracked ligaments and usually affects only the final part of the post-peak response.

Knowing the R-curve, one can easily calculate the load-point displacement u_c due to fracture [31, 45, 50]. Let u_0 = displacement calculated from elasticity as if there were no crack, and $u = u_c + u_0$ = the total displacement. One determines first the total complementary energy, W_P,

that would be released if the fracture occurred at constant load, P; from $\partial W_P/\partial a = bG = P^2 g(\alpha)/E'bd$, one gets

$$W_P = b\int_0^a G(a')\,da' = \frac{P^2}{E'b}\int_0^\alpha g(\alpha')\,d\alpha'. \tag{21}$$

According to Castigliano's theorem,

$$u_c = \frac{\partial W_P}{\partial P} = \frac{2P}{E'b}\int_0^\alpha g(\alpha')\,d\alpha'. \tag{22}$$

At the same time, from (5) for $G = R$:

$$P = b\sqrt{\frac{E'd}{g(\alpha)}R(c)}. \tag{23}$$

Choosing various values of α, one can calculate u_c and P from (22) and (23), which defines the load-deflection curve parametrically. As for u_0, it need not be calculated for our purpose since the elastic part of deformation dissipates no energy.

4. Calculation of the work-of-fracture from the *R*-curve

As we have seen, from the size effect law one can determine the R-curve, and from the R-curve one can calculate the diagram of the load vs. the load-point displacement. Thus, the work-of-fracture can be calculated from (1), or directly from the R-curve [16] (see Fig. 1c):

$$W_f = \int_0^l R(c)\,dc. \tag{24}$$

Let now the R-curve, obtained as the envelope of fracture equilibrium curves of all sizes (and approximated by (16)–(17)), be called the master R-curve. For a finite size specimen, the master R-curve is followed only up to the peak load, i.e. through the regime in which the fracture process zone is growing while remaining attached to the notch tip (we of course consider only specimens for which $g'(\alpha) > 0$). Up to the peak load, the elastic zone surrounding the fracture process zone is opening up, because the effective stress intensity factor grows. After the peak load (beginning approximately but not exactly at the peak load), this factor ceases to grow, and the elastic zone around the fracture process zone ceases to open up further. Thus, after the peak load, the fracture process zone detaches itself from the notch tip and, as an approximate picture, travels forward without growing any more.

In view of this picture, the energy required for crack growth after the peak load must be kept constant and equal to the value of the master R-curve at the peak load [31], as shown in Fig. 1c. This has been verified by fitting of experimental load-deflection curves for rock [31] as well as high-strength concrete [32]. An important point is that the location of the point c_p at which

R becomes constant, i.e. the peak-load point, depends on specimen size d. Thus, the R-curve actually followed is different for each size and coincides with the master R-curve only during the load ascent up to the peak load.

Remark: The constancy of R after the peak load of course must cease to hold (and the R-value must start to decrease) as the crack front approaches the end of the ligament, because the boundary interference will tend to diminish the fracture process zone size. We exclude the terminal behavior from consideration and assume that it plays only a minor role.

The work-of-fracture may now be divided into two parts, W_1 and W_2, corresponding to the rising R-curve for the pre-peak regime, and to the horizontal portion for the post-peak regime (Fig. 1c):

$$W_f = W_1 + W_2, \tag{25}$$

in which

$$W_1 = b\int_0^{c_p} R(c)\,\mathrm{d}c, \quad W_2 = R(c_p)b(l - c_p). \tag{26}$$

For size d and at the peak load, one gets from (19) the effective relative crack length, α_p. From this, the effective length of the fracture process zone is $c_p = (\alpha_p - \alpha_0)d$. Then one can write

$$W_1 = b\int_{\alpha_m}^{\alpha_p} R(c)\frac{\mathrm{d}c}{\mathrm{d}\alpha'}\,\mathrm{d}\alpha', \tag{27}$$

in which from (17)

$$\frac{\mathrm{d}c}{\mathrm{d}\alpha} = -\frac{g'(\alpha_0)}{g(\alpha_0)}\frac{g(\alpha)\,g''(\alpha)}{[g'(\alpha)]^2} \tag{28}$$

and the value of α at $c = 0$ is given [34] by

$$\alpha_m = \alpha_0 + \frac{g(\alpha_m)}{g'(\alpha_m)}. \tag{29}$$

Finally

$$W_1 = bG_f c_f \frac{g'(\alpha_0)}{g(\alpha_0)}\bar{W}_1, \quad \bar{W}_1 = \frac{1}{g(\alpha_0)}\int_{\alpha_p}^{\alpha_m}\left[\frac{g(\alpha)}{g'(\alpha)} - (\alpha - \alpha_0)\right]\frac{g(\alpha)g''(\alpha)}{g'(\alpha)}\,\mathrm{d}\alpha, \tag{30}$$

$$W_2 = bG_f c_f \frac{g'(\alpha_0)}{g(\alpha_0)}\bar{W}_2, \quad \bar{W}_2 = \beta^2(1 - \alpha)(\alpha - \alpha_0)\frac{g'(\alpha)}{g(\alpha_0)}. \tag{31}$$

Thus, the fracture energy according to the work-of-fracture method used by RILEM is

$$G_f^R = \frac{W_1 + W_2}{bl} = G_f^{R_1} + G_f^{R_2}, \tag{32}$$

in which

$$G_f^{R1} = \frac{\bar{W}_1}{\beta(1-\alpha_0)} G_f, \quad G_f^{R2} = \frac{\bar{W}_2}{\beta(1-\alpha_0)} G_f. \tag{33}$$

In the foregoing derivation we assumed that all the nonlinearity arises from the fracture process zone. This implies that G_f^p (which represents $\lim G_f^R$ for $d \to \infty$) is equal to G_f according to Bažant's definition [1]. Furthermore, in the foregoing calculation we tacitly assumed that the master R-curve, determined only from peak-load states, is also applicable, as an approximation, to fracture propagation during ascending load. This assumption is corroborated by the success in correctly predicting the measured load-deflection curves.

For large sizes, the entire master R-curve (16) can be used, which simplifies the calculations. In this case W_1 and $\bar{W}_1$ are constants, obtained by substituting $c_p = c_f$ and $\alpha_p = \alpha_0$, in (26), (27), and (30); also W_2 is a linear function of $l = d(1 - \alpha_0)$, i.e.

$$W_2 = b(l - c_f)G_f. \tag{34}$$

Finally, considering (2) and (25) one gets the size effect relation suggested by Planas, Elices and co-workers (3). The parameter l_p in (3) is related to c_f by

$$l_p = \left(1 - \frac{g'(\alpha_0)}{g(\alpha_0)} \bar{W}_m\right) c_f, \tag{35}$$

in which $\bar{W}_m (= \bar{W}$ for $\alpha_p = \alpha_0)$ is a geometry function calculated from (30), So we may conclude that (3) of Planas and Elices can be used, as an approximation, for $\beta > \beta_m (l > c_f)$, where

$$\beta_m = \frac{g(\alpha_0)}{g'(\alpha_0)(1-\alpha_0)}. \tag{36}$$

The value of G_f^R which corresponds to β_m is

$$G_f^{Rm} = \frac{g'(\alpha_0)}{g(\alpha_0)} \bar{W}_m G_f. \tag{37}$$

But if (3) is used indiscriminately for $\beta < \beta_m$, discrepancy arises.

5. Size and shape dependence of fracture energy defined by work-of-fracture

Numerical results calculated from the foregoing equations for a three-point-bend fracture specimen with $\alpha_0 = \frac{1}{3}$ and the span-to-depth ratio $L/d = 2.5$ are plotted in Figs. 2–4 (the size is represented in terms of the nondimensional brittleness number, which is proportional to the beam depth). For this geometry, funtion $k(\alpha)$ was derived by finite element analysis and curve fitting [32] as

$$k(\alpha) = \frac{3L}{2d}\sqrt{\pi\alpha}(1-\alpha)^{-3/2}(1.0 - 2.50\alpha + 4.49\alpha^2 - 3.98\alpha^3 + 1.33\alpha^4). \tag{38}$$

Using this function, one can calculate $g(\alpha_0) = k^2(\alpha_0) = 14.20$, $g'(\alpha_0) = 2k(\alpha_0)k'(\alpha_0) = 72.71$, $\alpha_m = 0.4888$ (from (29)), $\bar{W}_m = 0.128$ (from (30) for $\alpha_p = \alpha_0$), $(l_p/c_f) = 0.343$ (from (35)), $\beta_m = 0.293$ (from (36)), and $G_f^{Rm}/G_f = 0.657$ (from (37).

Figure 2 shows the calculated ratios of the energy required for crack growth, i.e. the R-curve value from (16), and the apparent fracture energy G_c (11), both normalized by the (true) fracture energy, G_f, which represents the asymptotic value of the R-curve and is defined by extrapolation to infinite specimen size. The figure also shows the curve of the fracture energy according to RILEM work-of-fracture method, G_f^R, normalized to the true fracture energy, G_f (32).

An interesting observation may now be made: The RILEM fracture energy depends on the size of the specimen more than does the R-curve, while the opposite is desired from an ideal testing method.

Figures 3a and 3b show the curve of G_f^R/G_f for different relative notch depths, α_0, as function of $\bar{d}$ and d respectively. It is interesting to observe that, within a relatively broad range (Fig. 3a), namely $\frac{1}{3} \leqslant \alpha_0 \leqslant \frac{5}{6}$, the dependence of G_f^R on the intrinsic size $\bar{d}$ is nearly the same, while for a very short notch, such as $\alpha_0 = \frac{1}{6}$, this dependence becomes milder. On the other hand Fig. 3b shows strong dependence of G_f^R on the notch size for the same specimen size d.

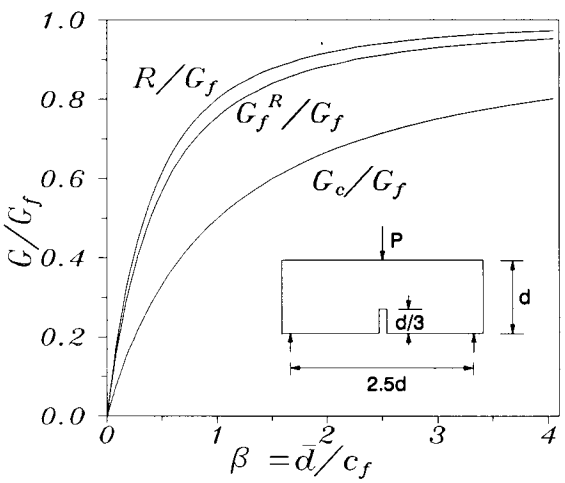

Fig. 2. Dependence of RILEM fracture energy G_f^R, relative to the true fracture energy G_f, on the specimen size characterized by brittleness number β, also the size dependence of the energy required for fracture growth, R, and apparent fracture energy, G_c, shown for comparison.

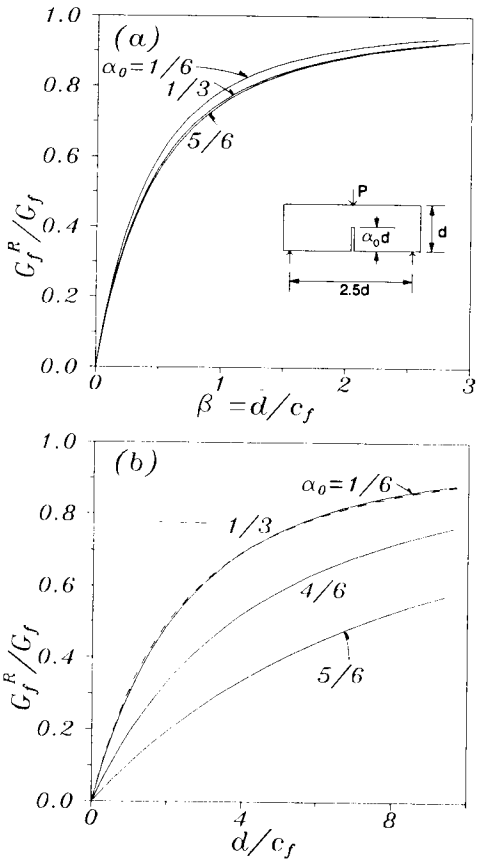

Fig. 3. Effect of relative notch depth $\alpha_0 = a_0/d$, on the value of RILEM fracture energy.

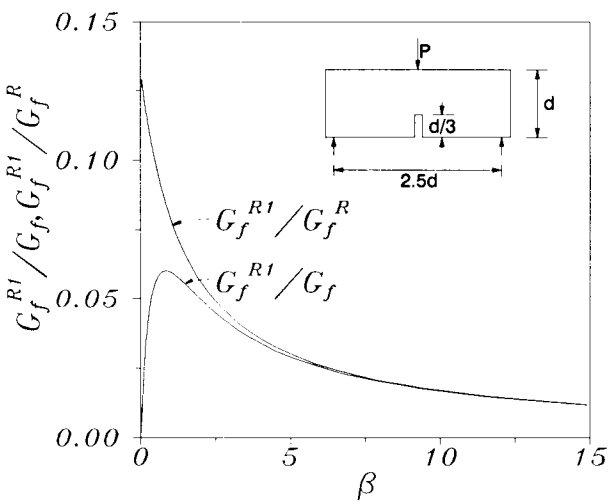

Fig. 4. Ratio of the pre-peak contribution to fracture energy, G_f^{R1}, to the RILEM fracture energy G_f^R and G_f.

Table 1. Analysis of test results of Maturana et al. [28]

T (°C)	E (GPa)	G_f^P (N/m)	G_f (N/m	κ_f
20	25.4	100	39	2.56
−10	27.2	227	87	2.61
−70	31.8	305	167	1.82
−170	47.9	332	316	1.05

It is of interest to determine the relative contributions of W_1 and W_2, (30) and (31), corresponding to the pre-peak and post-peak regimes. The pre-peak contribution of the work-of-fracture, G_f^{R1}, relative to the fracture energy, G_f, is plotted in Fig. 4 as a function of the specimen size, as characterized by the brittleness number β (33). We see that this ratio is generally rather small, always under 6 percent.

Figure 4 also shows the pre-peak contribution of the work-of-fracture relative to the fracture energy G_f^R according to the RILEM work-of-fracture method. This contribution decreases with increasing size from an initial value of about 13 percent.

The equivalence of G_f^P to G_f is true only theoretically, under the assumptions of the present analysis. The difference between G_f^P and G_f may be examined using the test results of Maturana, Elices and Planas [28] on saturated concrete at various low temperatures, presented in Table 1. The specimens have the same geometry as shown in Fig. 1, with the size range of $d = 50$–300 mm. The values of G_f^P are taken from [28–29] (calculated on the basis of (3)), and the values of G_f are estimated by nonlinear regression analysis based on (11) from the reported measured peak load values [28]. The moduli of elasticity used in the calculations of G_f are taken from uniaxial tension tests. As seen from the Table 1, G_f^P is much larger than G_f except for one case ($T = -170$°C). Figure 5 shows the dependence of G_f and G_f^P on temperature T, where a comparison is also made with the results from [51] on wet concrete at various elevated

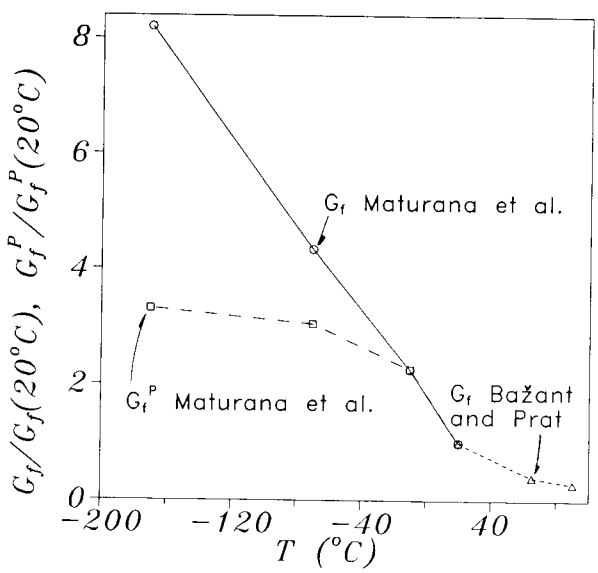

Fig. 5. Effect of temperature on fracture energy.

temperatures. The fracture energy values are normalized by the values corresponding to $T = 20°C$. It may also be of interest to note that the trend of G_f at low temperatures [28] is similar to that at high temperatures [51].

The ratio $\kappa = G_f^R/G_c$ indicates the degree of nonlinearity and ductility of the system [39], which again may depend on size and geometry. In the limit when $d \to \infty$, for which the nonlinearity due to fracture process zone is in theory eliminated, this ratio may be denoted as

$$\kappa_f = \frac{G_f^P}{G_f}. \tag{39}$$

If the extrapolation to infinity were exact, and if there were no dissipation nonlinearity sources outside the fracture process zone, one would have $\kappa_f = 1$. Practically, in most cases, $\kappa_f > 1$. The present theory predicts the RILEM fracture energy, G_f^R, to be always less than G_f in Bažant's definition. But this is contradicted by the results in Table 1 as well as many other places in the literature. This must be caused by some systematic errors, apart from random ones. Aside from a possible error in extrapolation to infinite size [36], one explanation might be that G_f^R is underestimated because dissipation sources outside the fracture process zone make a significant contribution to the total energy dissipation of the specimen. [6, 10, 21–22, 30, 52–53]. (For some geometries, e.g. simple unnotched tension specimens, this source of dissipation could yield a kind of size effect such that the apparent fracture energy based on the work-of-fracture increases with the specimen size [53].)

An important, spurious contribution to dissipation may come from the friction at the supports. As Planas and Elices [30] calculated, in order to make this contribution less than 1 percent of G_f^R, the friction coefficient of the rolling support in a three-point bend test would have to be below approximately 0.005L/d, which is not easy to achieve. For the wedge-splitting specimen with wedge angle 15°, the clamping force that the specimen exerts on the wedge requires the friction coefficient on the wedge to be below 0.0013 [30] if the friction contribution should be kept under 1 percent; this objective is next to impossible to attain in practice.

Figures 6 and 7 show variation of G_f^R with d (normalized by the G_f and d_0 values calculated from the size effect law) for a certain typical high strength concrete [32] and Indiana limestone [31], respectively. The data points are obtained from the area under the measured load-displacement diagram, (1) and (2). The curves in Figs. 6 and 7 show the variation of G_f^R predicted according to (32) from the observed dependence of peak nominal stress on the specimen size, (6) and (8). The comparisons are based on the modulus of elasticity obtained from the initial compliances of the fracture specimens rather than the standard tests on specimens. This yields mutually closer experimental (2) and predicted (32) values for G_f^R.

While the size effect method implies, for a given geometry, a unique pre-peak R-curve, because only one specimen size with the corresponding peak load corresponds to each $R(c)$-value, the R-curve to be used in the work-of-fracture method cannot be unique. The reason is that this method necessitates the R-values not only for all crack lengths but also for all specimen sizes; but the fracture process zone evolves probably differently in specimens of different notch lengths, not only in the post-peak regime but also in the pre-peak regime.

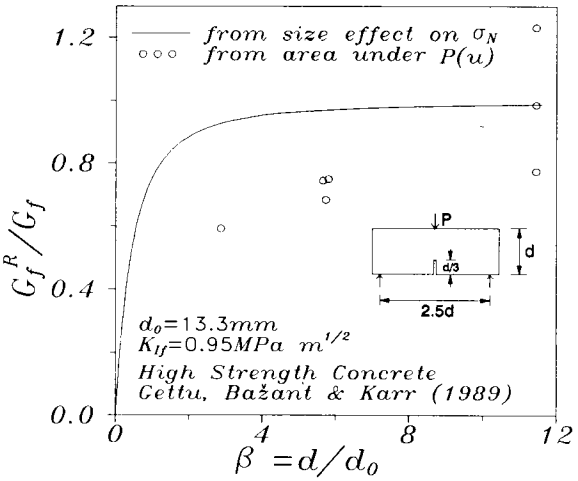

Fig. 6. Size dependence of G_f^R for high strength concrete [32].

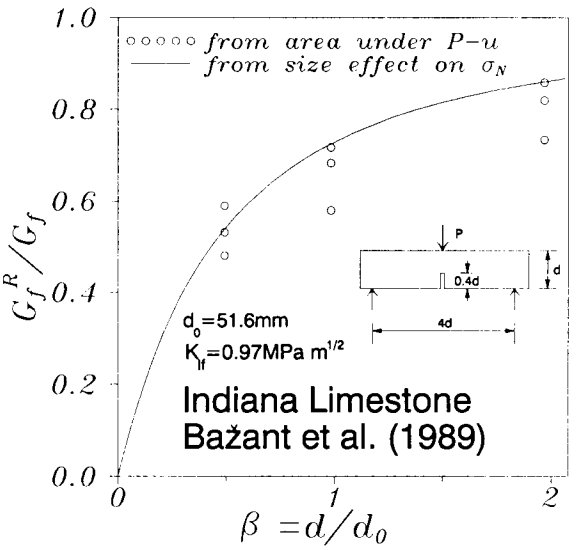

Fig. 7. Size dependence of G_f^R for Indiana limestone [31].

6. Conclusions

1. The basic premise of the present analysis is that although the size effect law of Bažant is approximate, it nevertheless has a broad range of validity, with an accuracy that is satisfactory compared to the inevitable scatter of test results. As shown in previous works, this law applies to the size range up to about 1:20, which suffices for most practical purposes. For a broader size range one would, of course, need a generalized size effect law, with additional parameters which would have to be geometry dependent; however, for the practical size range 1:20, such additional parameters are not needed, and the size effect law has the same form for various specimen shapes.

2. As a consequence of the aforementioned premise, the R-curve is geometry dependent, and may be calculated from size effect data on the maximum loads of fracture specimens of the same geometry. The R-curve can in turn be used to calculate the load-deflection curve and the work of fracture.

3. The calculations show that, in agreement with previous observations, the fracture energy defined by RILEM work-of-fracture method is not a constant but significantly increases with increasing specimen size. It is shown that the size dependence of the RILEM fracture energy is quite strong, in fact stronger than the size variation of the R-curve.

4. The calculations further show that (except for experimental scatter, dissipation outside the fracture process zone and other uncontrollable influences) extrapolation of the RILEM values of fracture energy to infinite specimen size must give exactly the same value of fracture energy for an infinitely large specimen as does the size effect method.

5. The contribution of the pre-peak work of fracture to the total fracture energy is rather small, and decreases with increasing specimen size.

6. As a by-product of the analysis, the fracture energy acording to the RILEM work-of-fracture method is seen to be sensitive to the relative notch depth in a three-point-bend test.

Acknowledgments

Partial financial support for the size effect theory of an R-curve has been obtained from the Center for Advanced Cement-Based Materials at Northwestern University (NSF grant DMR-8808432), and for the study of the RILEM method of determining the fracture energy from NSF Grant BSC-8818239 to Northwestern University. The previous research of the size effect in fracture was funded under AFOSR grant 91-0140 and contract F49620-87-C-0030DEF with Northwestern University. The second author wishes to express his thanks for a scholarship he received from Sharif University of Technology, Tehran, Iran.

References

1. Z.P. Bažant, in *Fracture of Concrete and Rock, Proceedings of SEM-RILEM International Conference*, Houston, June, 1987, S.P. Shah and S.E. Swartz (eds.), Springer-Verlag, NY (1989) 229–241; also Preprints, published by Society for Experimental Mechanics (1987) 390–402.
2. Z.P. Bažant and P.A. Pfeiffer, *ACI Material Journal* 84 (6) (1987) 468–480.
3. Z.P. Bažant, *Journal of Engineering Mechanics, ASCE* 110 (4) (1984) 518–35.
4. Z.P. Bažant, in *Proceedings of U.S.–Japan Seminar*, Tokyo, 1985, *Finite Element Analysis of Reinforced Concrete Structures*, C. Meyer and H. Okamura (eds.), ASCE, New York (1986) 121–150.
5. RILEM, *Materials and Structures* 18 (106) (1985) 285–290.
6. A. Hillerborg, *Materials and Structures* 18 (106) (1985) 291–96.
7. J. Nakayama, *Journal of American Ceramics Society* 48 (11) (1965) 583–87.
8. H.G. Tattersall and G. Tappin, *Journal of Material Science* 1 (3) (1966) 296–301.
9. A. Hillerborg, *Materials and Structures* 18 (107) (1986) 407–13.
10. P.E. Petersson, *Cement and Concrete Research* 10 (1) (1980) 78–101.
11. F. Moavenzadeh and R. Kuguel, *Journal of Materials* 4 (3) (1969) 497–519.
12. F. Radjy, *Cement and Concrete Research* 3 (4) (1973) 343–361.
13. A. Hillerborg, M. Modéer and P.-E. Petersson, *Cement and Concrete Research* 6 (6) (1976) 773–782.
14. M.P. Wnuk, *Journal of Applied Mechanics* 41 (1) series E (1974) 234–42.
15. A. Bascoul, F. Kharchi and J.C. Maso, in *Fracture of Concrete and Rock, Proceedings of SEM-RILEM International Conference*, Houston, June 1987, S.P Shah and S.E. Swartz (eds.) Springer-Verlag, NY (1989) 396–408.
16. M. Sakai, K. Urashima and M. Inagaki, *Journal of American Ceramics Society* 66 (12) (1983) 868–74.

17. T.B. Troczynski and P.S. Nicholson, *Journal of American Ceramics Society* 70 (2) (1987) 78–85.
18. F.H. Wittmann, K. Rokugo, E. Brühwiler, H. Mihashi and P. Simonin, *Materials and Structures* 21 (121) (1988) 21–32.
19. E. Brühwiler and F.H. Wittmann, *Engineering Fracture Mechanics* 35 (1/2/3) (1990) 117–25.
20. F.H. Wittmann, H. Mihashi and N. Nomura, *Engineering Fracture Mechanics* 35 (1/2/3) (1990) 107–15.
21. W. Brameshuber and H.K. Hilsdorf, *Engineering Fracture Mechanics* 35 (1/2/3) (1990) 95–106.
22. P. Nallathambi and B.L. Karihaloo, *Cement and Concrete Research* 16 (3) (1986) 373–82.
23. S.E. Swartz and T.M.E. Refai, in *Fracture of Concrete and Rock, Proceedings of SEM-RILEM International Conference*, Houston, June 1987, S.P. Shah and S.E. Swartz (ed.), Springer-Verlag, NY (1989) 242–254.
24. Y.S. Jenq and S.P. Shah, *Engineering Fracture Mechanics* 21 (5) (1985) 1055–1069.
25. S. XU and G. Zhao, in *Fracture Toughness and Fracture Energy, Test Methods for Concrete and Rock, Preprints of the Proceedings of an International Workshop*, Sendai, Japan, October, 1988, M. Izumi (ed.), Tohoku University, Sendai, Japan (1988) 48–62.
26. R.W. Davidge and G. Tappin, *Journal of Material Science* 3 (2) (1968) 165–73.
27. A. Hillerborg, in *Fracture Toughness and Fracture Energy, Test Methods for Concrete and Rock, Preprints of the Proceedings of an International Workshop*, Sendai, Japan, October 1988, M. Izumi (ed.), Tohoku University, Sendai, Japan (1988) 121–127.
28. P. Maturana, J. Planas and M. Elices, *Engineering Fracture Mechanics* 35 (4/5) (1990) 827–834.
29. J. Planas, P. Maturana, G. Guinea and M. Elices, in *Advances in Fracture Research, Proceedings of an International Conference (ICF7, Vol. 2)*, Houston, March 1989, Salama et al (eds.), Pergamon Press, Oxford (1989) 1890–1817.
30. J. Planas and M. Elices, in *Fracture Toughness and Fracture Energy, Test Methods for Concrete and Rock, Preprints of the Proceedings of an International Workshop*, Sendai, Japan, October, 1988, M. Izumi (ed.), Tohoku University, Sendai, Japan (1988) 1–18.
31. Z.P. Bažant, R. Gettu and M.T. Kazemi, *International Journal of Rock Mechanics and Mining Sciences* 28 (1991) 43–51.
32. R. Gettu, Z.P. Bažant and M.E. Karr, Fracture Properties and Brittleness of High Strength Concrete, Report No. 89-10/B627f, Center for Advanced Cement-Based Materials, Northwestern University (1989); also *ACI Materials Journal*, in press.
33. H. Tada, P.C. Paris and G.R. Irwin, *The Stress Analysis of Cracks Handbook*, 2nd. ed., Paris Production, St. Louis (1985).
34. Z.P. Bažant and M.T. Kazemi, *International Journal of Fracture* 44 (1990) 111–131.
35. Z.P. Bažant, and M.T. Kazemi, *Journal of American Ceramics Society* 73 (1990) 1841–1853.
36. J. Planas and M. Elices, in *Cracking and Damage, Strain Localization and Size Effect*, Proceedings of France-US Workshop, Cachan, France, 1988. J. Mazars and Z.P. Bažant (eds.), Elsevier, London (1989) 462–476.
37. H. Horii, Z. Shi and S.-X. Gong, in *Cracking and Damage, Strain Localization and Size Effect*, Proceedings of France-US Workshop, Cachan, France, 1988, J. Mazars and Z.P. Bažant (eds.), Elsevier, London (1989) 104–115.
38. Z.P. Bažant, and Y. Xi, Statistical Size Effect in Quasibrittle Structures: II. Nonlocal Theory, Report No. 90-5/616s(II), Center for Advanced Cement-Based Materials, Northwestern University, Evanston, Ill., 1990; also *Journal of Engineering Mechanics, ASCE*, in press.
39. J. Homeny, T. Darroudi and R.C. Bradt, *Journal of American Ceramics Society* 63 (5–6) (1980) 326–31.
40. A. Carpinteri, *International Journal of Solids and Structures* 25 (4) (1989) 407–429.
41. P. Marti, *ACI Materials Journal* 86 (6) (1989) 597–601.
42. J.L. Shannon, Jr. and D.G. Munz, in *Chevron-Notched Specimens: Testing and Stress Analysis*, ASTM STP 855, J.H. Underwood et al. (eds.), ASTM, Philadelphia (1984) 270–280.
43. K. Matsuki, in *Fracture Toughness and Fracture Energy, Test Methods for Concrete and Rock, Preprints of the Proceedings of an International Workshop*, Sendai, Japan, October, 1988, M. Izumi (ed.), Tohoku University, Sendai, Japan (1988) 234–248.
44. J. Huang, and C. Li, *Composites* 20 (4) (1989) 361–378.
45. Z.P. Bažant, *Cement and Concrete Research* 17 (6) (1987) 951–967.
46. M. Ortiz, *International Journal of Solids and Structures* 24 (3) (1988) 231–250.
47. F. de Larrad, C. Boulay and P. Rossi, in *Utilization of High Strength Concrete*, Proceedings of a Symposium, Stavanger, Norway, June, 1987, I. Holand et al. (eds.), Tapir Publishers (1987) 215–223.
48. Z.P. Bažant, J.-K. Kim and P.A. Pfeiffer, *Journal of Structural Engineering* 112 (2) (1986) 289–307.
49. Z.P. Bažant, S.-G. Lee and P.A. Pfeiffer, *Engineering Fracture Mechanics* 26 (1) (1987) 45–57.
50. M. Sakai and M. Inagaki, *Journal of American Ceramic Society* 72 (3) (1989) 388–394.
51. Z.P. Bažant and P.C. Prat, *ACI Materials Journal* 85 (4) (1988) 262–271.
52. L.J. Malvar and G.E. Warren, *Materials and Structures* 20 (120) (1987) 440–447.
53. M. Elices and J. Planas, in *Fracture Mechanics of Concrete Structures*, RILEM TC90-FMA, L. Elfgren (ed.), Chapman and Hall, London (1989) 16–66.